Spectrochimica Acta Part A: Molecular and Biomolecular Spectroscopy 297 (2023) 122695

Contents lists available at ScienceDirect

Spectrochimica Acta Part A:
Molecular and Biomolecular Spectroscopy

journal homepage: www.journals.elsevier.com/spectrochimica-acta-part-a-molecular-and-biomolecular-spectroscopy

Luminescence properties of Ln^{3+} doped $BaMoO_4$ (Ln^{3+} = Sm^{3+} and Dy^{3+}) phosphors under UV excitation

Ch. Victory Devi [a,*], N. Rajmuhon Singh [b]

[a] Department of Chemistry, PUC, Mizoram University, Aizawl 796001, Mizoram, India
[b] DM University, Imphal 795001, India

HIGHLIGHTS

- Tuning of intensity on varying the concentration of Ln^{3+} ions(Ln^{3+} = Sm^{3+} and Dy^{3+})
- No change on the structural properties of host $BaMoO_4$ on doping Ln^{3+} ions,
- Sm^{3+}- doped $BaMoO_4$ phosphors emit strong orange–red and $BaMoO_4$:Dy^{3+} emits greenish-yellow light.
- Redispersible Ln^{3+}-doped $BaMoO_4$ in polar solvents.
- Emission of intense yellow color by incorporating Dy^{3+} doped $BaMoO_4$ in thin polymer film.

GRAPHICAL ABSTRACT

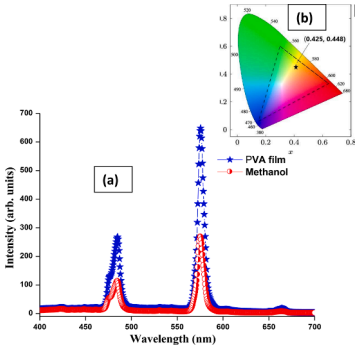

ARTICLE INFO

Keywords:
Tetragonal
Scheelite structure
Microcrystal, Greenish-orange emitting
Phosphor

ABSTRACT

Ln^{3+} doped $BaMoO_4$ (Ln^{3+} = Sm^{3+} and Dy^{3+}) nanoparticles have been synthesized successfully using ethylene glycol as a solvent. All the prepared samples are well indexed into the pure scheelite-type tetragonal structure of $BaMoO_4$, the doping of trivalent ions (Ln^{3+}) in to the bivalent host ions (Ba^{2+}) sites of the $BaMoO_4$ do not change the pure tetragonal structure of $BaMoO_4$ although there is a charge difference between Ba^{2+} and Ln^{3+}. The SEM image of the prepared $BaMoO_4$ samples shows a number of uniform shuttle-like nanocrystalline with protrusion in the middle. The doping of Ln^{3+} ions do not change the morphology of the $BaMoO_4$. The photoluminescence study has been carried in detail by measuring the excitation and emission spectra of the prepared samples. The excitation spectrum consists of a broad band with a maximum at about 268 nm thereby demonstrating the transfer of energy from MoO_4^{2-} groups to the doped Ln^{3+} ions. Yellow emission is dominated over blue in case of Dy^{3+} doped $BaMoO_4$ and in Sm^{3+} doped $BaMoO_4$ red emission dominated over other lights under UV excitation. The luminescence intensity is highest at 10 at.% Ln^{3+} under the UV excitation. Under this UV excitation $BaMoO_4$:Sm^{3+} exhibits strong orange-red and $BaMoO_4$:Dy^{3+} greenish-yellow emissions. Excitation of Dy^{3+} in thin film of $BaMoO_4$ emits an intense yellow color which could be applicable in the field of biological assays and biological fluorescence labeling.

* Corresponding author at: Department of Chemistry, PUC, Mizoram University, Aizawl 796001, Mizoram, India.
E-mail addresses: chvictory19@gmail.com (Ch. Victory Devi), rajmuhon@gmail.com (N. Rajmuhon Singh).

https://doi.org/10.1016/j.saa.2023.122695
Received 21 October 2022; Received in revised form 23 March 2023; Accepted 30 March 2023
Available online 3 April 2023

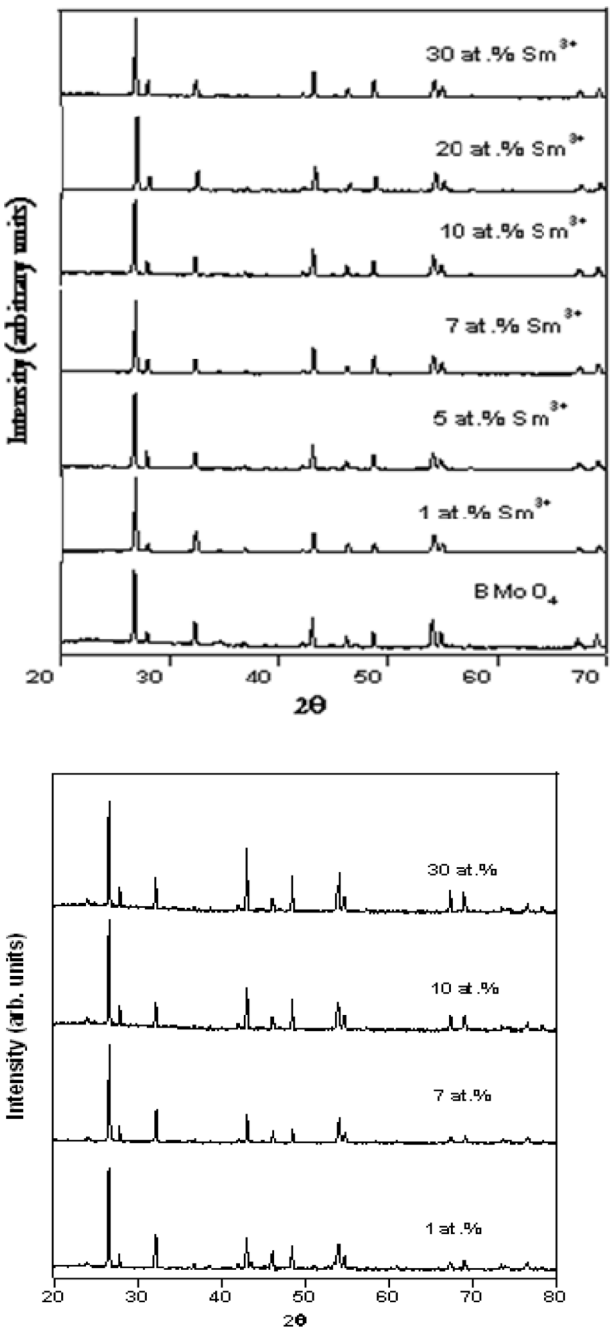

Fig. 1. XRD pattern of (a) Sm^{3+}-doped $BaMoO_4$ and (b) Dy^{3+}-doped $BaMoO_4$ (Sm^{3+}/Dy^{3+} = 1, 3, 5, 7, 10, 20 and 30 at.%) nanoparticles.

1. Introduction

Luminescence nanomaterials have been given considerable interest in the last few years because of their advanced applications in opto-electronic devices [1–5]. Particularly, the photoluminescence properties of such materials are influenced highly by the particle shape and size of the materials [6,7]. This intrinsic properties of nanocrystals are concerned with today's developing applications of nanotechnology leading to the designing of new devices. Therefore, the fabrication of nanomaterials with fascinating hierchical architectures are highly demanded due to well-controlled morphologies, dimensionality, desired chemical properties and is remained as one of the most challenging issues today. Recently developed conventional solid state reaction method need high annealing temperature and carbonate materials for their synthesis, therefore synthesized materials have irregular morphologies and abnormal grain size, [8]. In order to overcome such difficulties different synthesis methods such as sol–gel processes, precipitation, combustion, microemulsion, and chemical vapor technique have been studied to synthesize the inorganic functional materials. Among these methods co-precipitation method using ethylene glycol as a capping agent is found to be very simple, cheap and versatile process for the synthesis of various inorganic materials with diverse morphologies and architectures. In this synthesis method EG act as a stabilizer to regulate the nucleation process, particle growth and morphology of the nanoparticles, and also acts a capping agent to remove agglomeration of particles which hampers the luminescent intensity.

In the present paper, we have synthesized shuttle-like Ln^{3+} (Ln^{3+} = Sm^{3+} and Dy^{3+}) doped $BaMoO_4$ nanoparticles via co-precipitation method. In this method ethylene glycol was used as a capping agent as well as a solvent. Co-precipitation method is more advantageous over other conventional methods as all the samples are prepared at low temperature and required short refluxing time and mostly environmentally friendly. Molybdates with scheelite crystal structure, $AMoO_4$ (A = Ca, Ba and Sr) are considered as potential host for matrix of lanthanide activators because of their unique structure, superior chemical stability and prominent luminescence properties [9–12]. Among these molybdates $BaMoO_4$ is considered to be an excellent host for trivalent lanthanide ion activators[9–10,13,14]. In $BaMoO_4$ structure, barium atoms are bonded to eight oxygens, forming $[Ba_2O_8]$ clusters with scalenohedral configuration [13,15]. And the central Molybdenum atoms are coordinated to four oxygens forming $[MoO_4]$ clusters. These $[MoO_4]$ clusters were able to induces six different bond angles of the O–Mo–O causing the displacement on a Mo atom (Fig. 5b). This MoO_4^{2-} cluster is bound loosely to Ba^{2+} cations, and with space group of $I4_1/a$ in C_64h symmetry. It plays an important role in exploring the luminescence activity of this host by absorbing excitation energy, then transferred to the activator thereby increasing the emission intensity of trivalent lanthanide ions [13,16]. The dopant trivalent lanthanide ions can occupy the host divalent Ba^{2+} sites with tetragonal symmetry. This motivates us to choose $BaMoO_4$ as host matrix in studying the luminescence properties of lanthanide ions. The luminescence properties of the as-prepared nanoparticles are studied in detail by correlating with the structure and morphology of the prepared samples and how its properties modified with change in structure and morphology are also discussed in the present paper. Trivalent lanthanide ions exhibit unique narrow emission band which could have been utilized in the development of displays devices. These materials showed high luminescence intensity on excitation under suitable wavelength. Trivalent dysprosium ions, Dy^{3+} is one of the potential activator which show strong luminescence exhibiting blue and yellow emission. In general, Dy^{3+} show three peaks corresponding to $^4F_{9/2} \rightarrow {}^6H_{15/2}$(blue) and $^4F_{9/2} \rightarrow {}^6H_{13/2}$ (Yellow) and $^4F_{9/2} \rightarrow {}^6H_{11/2}$ (red) transitions in emission spectra respectively. So, its emission color is close to white light under UV excitation which could be utilized in display devices. And Sm^{3+} ions also exhibits four main emission peaks at about 564, 600, 645 and 705 nm, corresponding to $^4G_{5/2}$–$^6H_{5/2}$ and $^4G_{5/2}$–^6H_J (J = 7/2, 9/2, 11/2) transitions respectively.

2. Experimental

2.1. Sample preparation

The $BaMoO_4$: Sm (Sm^{3+} = 1, 3, 5, 7, 10, 20 and 30 at%) and $BaMoO_4$: Dy^3 (Dy^{3+} = 1, 3, 5, 7, 10, 20 and 30 at%) nanoparticles are prepared via glycole route at low temperature. For a typical preparation of 5 at.% Sm^{3+}- doped $BaMoO_4$ nanoparticles, 0.25 g of $Ba(NO_3)_2$ and 0.0223 g of $Sm(NO)_3$ are taken and dissolved in concentrated nitric acid (HNO_3). Ethylene glycol was used as capping agent. Then the solution was heated to remove excess acid. Required amount of $NaMoO_4$ is added and ethylene glycol (EG) were added. NaOH was used to maintain the pH of

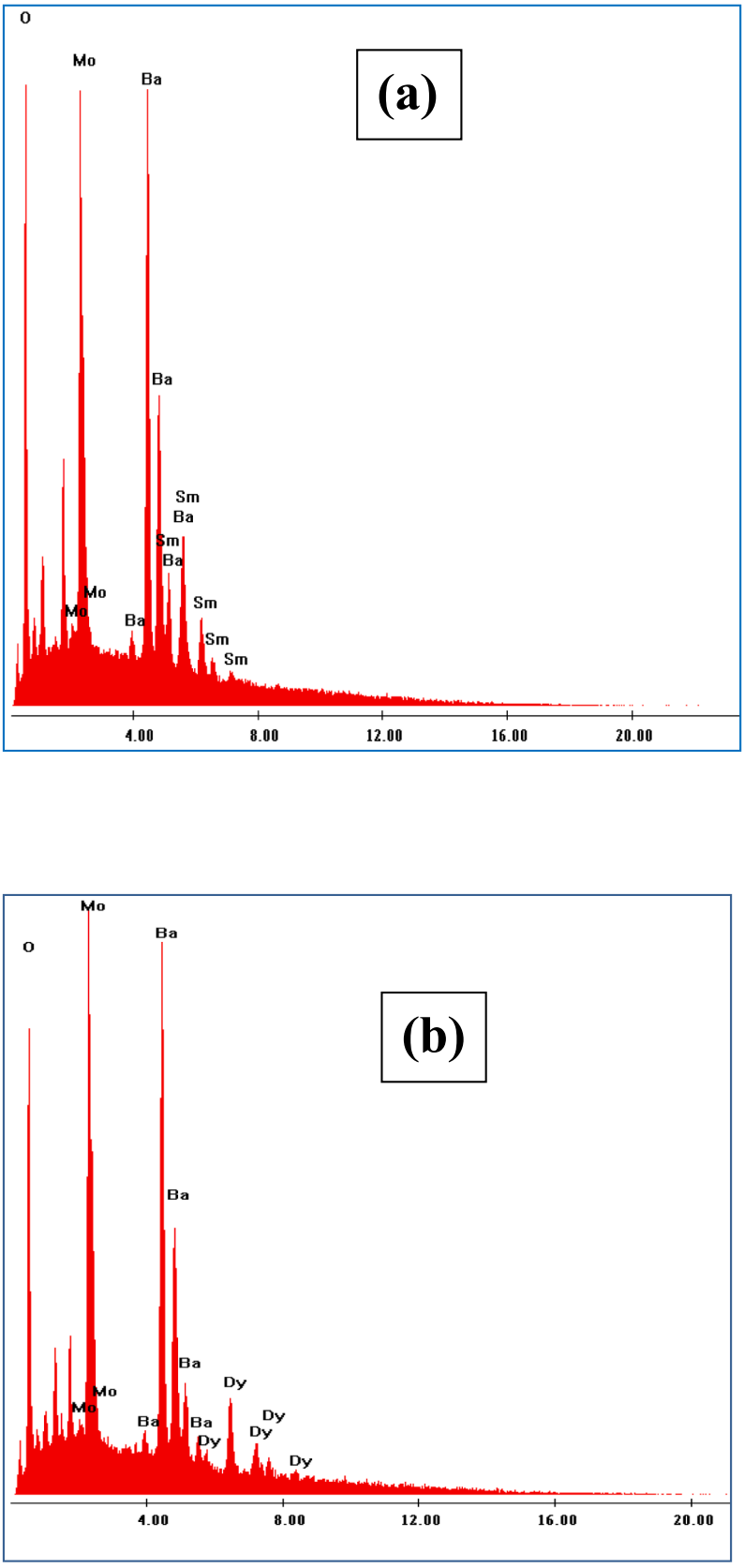

Fig. 2. EDX pattern of 20 at.% (a) Sm^{3+}- and (b) Dy^{3+} -doped $BaMoO_4$.

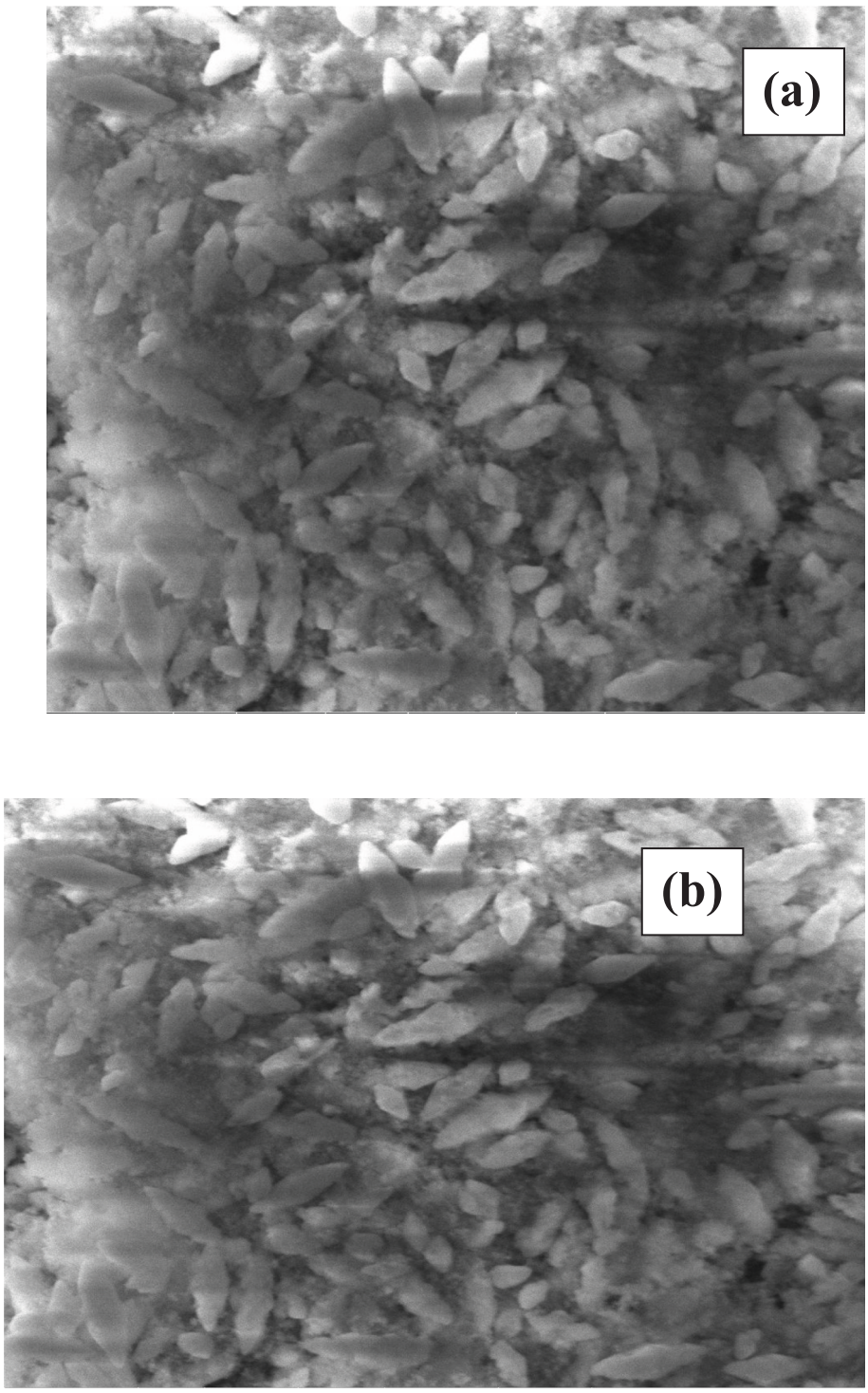

Fig. 3. SEM image of 20 at.% (a) Sm^{3+} and (b) Dy^{3+} –doped $BaMoO_4$.

the solution. The solution mixture was then refluxed for 3 hrs at ~120-150^{O}C and stirred continuously till the formation of white precipitates. During the nucleation a number of small aggregates called nucleus are formed which then growth to form the precipiate of suffiuciently large particle size. The obtained precipitate was separated by centrifugation, washed with ethanol and then acetone to remove the excess of EG, and then dried at room temperature for analyzing the samples.

2.2. Measurement techniques

Powder X-ray diffraction (XRD) patterns of all samples are recorded using PANalytical powder diffractometer (X'Pert PRO) with CuKα (1.5405 *Å*) radiation with Ni filter. Nanocrystalline nature of the samples are studied using Scanning electron microscope (SEM,) recorded by FEI Quanta 250 equipped with an energy dispersive X-ray spectroscopy. Fourier transform infrared (FTIR) spectra were taken on a Shimadzu (8400S) using a KBr pellet technique. The average crystallizes size of all the prepared samples are calculated using Scherrer's formula. The

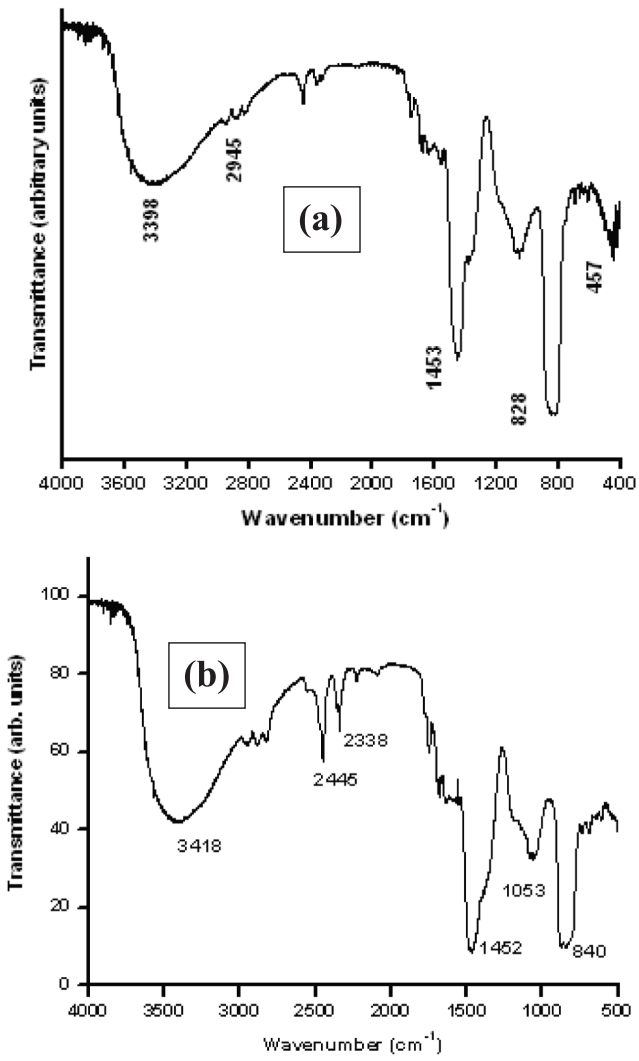

Fig. 4. FT-IR spectra of 7 at.% (a) Sm^{3+}- and (b) Dy^{3+} -doped $BaMoO_4$.

photoluminescence of the samples are studied by measuring the emission and excitation spectra, and decay lifetimes on Perkin Elmer (LS-55) instrument with a Xe discharge lamp. All the measurements of the samples are taken at room temperature.

3. Results and discussions

3.1. XRD study

Fig. 1 Shows the XRD pattern of all the prepared Sm^{3+}-doped $BaMoO_4$ and Dy^{3+} doped $BaMoO_4$ (Sm^{3+}/Dy^{3+} = 1, 3, 5, 7, 10, 20 and 30 at.%). All the samples are well crystallized into the pure tetragonal scheelite-type structure of barium molybdate ($BaMoO_4$) (JCPDS No. 29–0193, Space group: $I41/a$, No. 88). No other peaks are found thereby showing the formation of pure tetragonal phase of $BaMoO_4$. This indicates the substitution of Sm^{3+} /Dy^{3+} ions in Ba^{2+} sites. As well, the charge difference between the activator trivalent ions (Dy^{3+} and Sm^{3+}) and bivalent host ions (Ba^{2+}) do not cause any change in the structural properties of the $BaMoO_4$.. The average crystallize size of the particles are calculated by Debye's Scherrer formula

$$D = 0.9\lambda/\beta\cos\theta \quad (1)$$

Where λ is the wavelength of the X-ray used, θ is the diffraction angle of the most intense diffraction peak (112), and β is full width half maxima (FWHM) of the peak. The average crystallite size for the prepared Sm^{3+}- doped samples are found in the range of 32–55 nm and that of Dy^{3+} doped samples lies in the range of 35–62 nm respectively. The XRD peaks are sharp and strong showing that a nanoparticle of single phase with high crystallinity can be synthesized successfully by our simple methods. And the intensity of the diffracted peaks of Sm^{3+}-doped $BaMoO_4$ and Dy^{3+} -doped $BaMoO_4$ increase with Sm^{3+}/Dy^{3+} concentration. The ionic radii of Sm^{3+} and Dy^{3+} (1.03 Å) are lower than that of the host ion Ba^{2+} (1.42 Å). So, when the smaller ionic radii Sm^{3+}/Dy^{3+} ions occupy the Ba^{2+} ions in $BaMoO_4$ host lattice the crystal cell parameters decreases leading to the contraction of unit cell volume. Therefore, the diffraction peaks of the Sm^{3+}-doped $BaMoO_4$ and Dy^{3+} -doped $BaMoO_4$ are found to be shifted slightly towards higher angle with respect to the position of standard $BaMoO_4$ (JCPDS No. 29–0193, space group: $I41/a$, No. 88). And this observed small shifting of diffraction peaks is due to the low at.% of doping ions Sm^{3+}/Dy^{3+} into the host.

3.2. EDX

The chemical composition of the prepared samples are studied by taking the energy dispersive X-ray (EDX) spectrum. The Fig. 2a shows the EDX spectra of Sm^{3+}-doped $BaMoO_4$. Only Ba, Mo, O and Sm signals are present in EDX spectrum confirming formation of a pure phase of $BaMoO_4$:Sm^{3+}. And the EDAX spectra of Dy-doped $BaMoO_4$ also as shown in Fig. 2b shows peaks of Ba, Mo and O signals and the Dy signals confirming the formation of a pure phase of $BaMoO_4$:Dy^{3+} nanocrystals.. Additional peaks of Na or C signals were not present in the EDX spectrum thereby supporting effectively the XRD data of the sample.

3.3. SEM study

SEM measurements were carried out to study the morphology of the prepared phosphors. Fig. 3a and Fig. 3b show the SEM images of $BaMoO_4$:20Sm^{3+} and $BaMoO_4$:20Dy^{3+} phosphors. The doping of small amounts of Dy and Sm into $BaMoO_4$ host does not produce change in the phase, crystallization and morphology of the host. SEM images showed a number of relatively uniform shuttle-like nanocrystals with tips and protrusions in the middle.

3.4. FT-IR study

Fig. 4a and 4b showed the IR spectra of 5 at.% Sm^{3+}-doped $BaMoO_4$ and $BaMoO_4$:5Dy^{3+} sample. The appearance of broad peak around 3398 cm^{-1} and weak band at 1651 cm^{-1} are attributed to O—H stretching vibration and H—O—H bending vibration in H_2O absorbed on the surface of the samples [17]. The additional bands appeared at 2876 cm^{-1} and 2945 cm^{-1} are due to adsorbed EG molecules on the surface of the samples [17]. The strong band at 1453 cm^{-1} is due to the presence of nitrate. The intense IR band observed at 828 cm^{-1} is due to F_2 (ν_3) antisymmetric stretching vibration of Mo–O bond in MoO_4^{2-} tetrahedron [18,19] which confirm the presence of MoO_4^{2-} groups in the sample. It gives the additional proof for the formation of the $BaMoO_4$ product, supporting well the XRD and EDX data. Here it would be worthwhile to mention that FT-IR spectra of Ln^{3+}-doped $BaMoO_4$ (Ln^{3+} = Sm^{3+} and Dy^{3+}) samples are identical to that of pure $BaMoO_4$ sample.

3.5. Photoluminescence study

Fig. 5a and 5b show the excitation spectra of $BaMoO_4$:Sm^{3+} and $BaMoO_4$:5Dy^{3+} sample under the emission wavelength at 646 nm. A broad band was observed in the wavelength range of 225–300 nm which can be assigned due to charge transfer from the 2p orbitals of the oxygen atom to the 4d orbitals of the molybdenum atom [20–22]. This is also due to the intervalence charge transfer from the ground state 4f orbitals

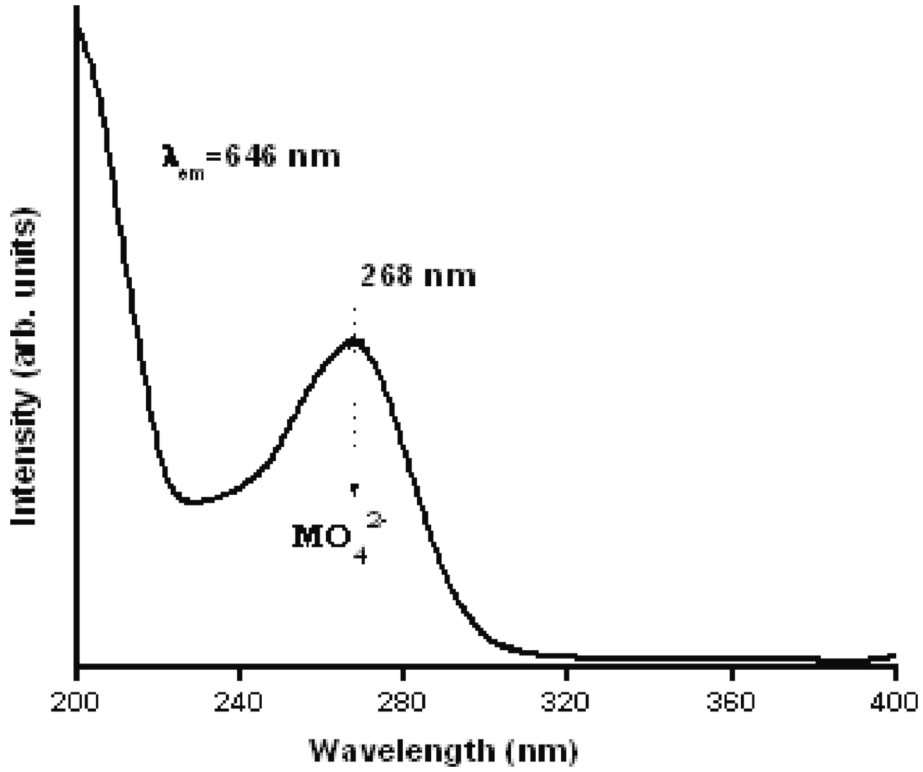

Fig. 5. Photoluminescence excitation spectra of prepared $BaMoO_4$ nanoparticle.

of Sm^{3+}/Dy^{3+} to the Mo^{6+} inside the MoO_4^{2-} groups inducing energy band at somewhate lower energy in comparison to the interband excitation due to the host lattice [23,24]. And finally CTB is due to the transfer of electrons from the completely filled 2p orbitals of the O^2 anion to the partially filled 4f orbitals of the Sm^{3+}/Dy^{3+} [22,24,25]. The appearance of this broad band with maximum at 268 nm shows the efficient transfer of energy from MoO_4^{2-} groups to the Sm^{3+} /Dy^{3+} ions and the excitation of the Sm^{3+}/Dy^{3+} ions is mainly through the energy transfer from the MoO_4^{2-} groups to Sm^{3+}/Dy^{3+} ions.

The emission spectrum of $BaMoO_4$:Ln^{3+} (Ln = Sm^{3+}/ and Dy^{3+}) sample was obtained on excitation at 268 nm into the MoO_4^{2-} groups. The emission spectra of Sm^{3+} doped $BaMoO_4$ (Fig. 6a) consists of four main peaks due to $^4G_{5/2}$–$^6H_{5/2}$ and $^4G_{5/2}$–^6H_J (J = 7/2, 9/2, 11/2) transitions at about 564, 600, 645 and 705 nm, respectively. The emission spectra of Dy^{3+} obtained on excitation under 268 nm also consist of magnetic dipole transition $^4F_{9/2} \rightarrow {}^6H_{15/2}$ at 482 nm (blue), electric dipole transition $^4F_{9/2} \rightarrow {}^6H_{13/2}$ at 575 nm (yellow) and weak $^4F_{9/2} \rightarrow {}^6H_{11/2}$ transition at 668 nm (red) (Fig. 6b). Generally, the yellow light is emitted when the Dy^{3+} is located at low symmetry environment without inversion centre while the blue emission is stronger when Dy^{3+} is located in high symmetry with an inversion center. However in our present study, the emission spectra of both Sm^{3+} and Dy^{3+} are dominated by an electric-dipole transition over other transitions indicating that Sm^{3+}/Dy^{3+} occupy environment without the inversion centre and is very sensitive to the environment. This can be understood from the fact the ionic radius of Sm^{3+} and Dy^{3+} (1.03 Å) are lower than that of the host ion Ba^{2+} (1.42 Å for Ba^{2+} ion) but much larger than Mo^{6+} ionic radius (0.41 Å) of the MoO_4^{2-} cluster. So, Ba^{2+} coordinated with eight oxygen atoms with S_4 space group in non-inversion symmetry site was observed in $BaMoO_4$ structure. From this discussion, it confirms that Sm^{3+}/Dy^{3+} ions occupy the Ba^{2+} ions and the emission is purely from the dopant Sm^{3+}/Dy^{3+} ions.

The symmetry of Sm^{3+}/Dy^{3+} in $BaMoO_4$ can be explained in terms of Asymmetric ratio (A_{21}) which is defined as the ratio of intensity of electric dipole transition to that of magnetic dipole transition.

$$A_{21} = \frac{\int_{560}^{590} I_2 d\lambda}{\int_{460}^{500} I_1 d\lambda} \quad (2)$$

Where I_1 and I_2 represent the respective integrated intensity of $^4F_{9/2} \rightarrow {}^6H_{13/2}$ and $^6H_{15/2}$ transitions of Dy^{3+}, respectively. Higher is the Asymmetric ratio, the lower is the site of symmetry occupied by Sm^{3+}/ Dy^{3+} ions. The asymmetric ratio, thus gives the picture of the local environment around the Sm^{3+}/Dy^{3+} ions. The asymmetric ratio (A_{21}) is greater than unity (≈1.81) in our study thereby showing the dominance of electric dipole transition over magnetic dipole transition. It further reveals the low symmetry around Sm^{3+}/Dy^{3+}.

The emission intensity of Sm^{3+}/Dy^{3+} increases with the increase in concentration from 1 to 10 at.% and then decreases on further increasing Sm^{3+}/Dy^{3+} content. Increasing Sm^{3+}/Dy^{3+} concentrations reduces the intensities of Sm^{3+}/ Dy^{3+}, due to the phenomenon of luminescence quenching. At low at.% of Sm^{3+}/Dy^{3+} ion, the distance between the Ln and Ln ions was increased and no cross relaxation process occurs between the Ln^{3+} ions. That means, there occurs charge transfer from the 2p state of the oxygen atom to the 4d states of the Mo. However, on further increasing Ln^{3+} ion concentration, the mean distance between the Ln^{3+} ions become less than the critical value then the cross relaxation process between them increased, which leads to low emission of Ln^{3+}. Critical value is dependent on crystal structure of host, particle size as well as type of doped lanthanide ions.

The integrated area under emission peaks of $^4G_{5/2}$–$^6H_{9/2}$ and $^6H_{7/2}$ has been calculated to study the change in luminescence intensity of Ln^{3+} doped $BaMoO_4$ nanoparticles with Ln^{3+} ions using the Gaussian distribution function, eqn (3):

$$I = I_0 + \sum_{i=1}^{2} \frac{A_i}{w_i\sqrt{\pi/2}} e^{2(\lambda-\lambda_{ci})^2/w_i^2} \quad (3)$$

where I is the observed intensity, I_0 is the background intensity, w_i

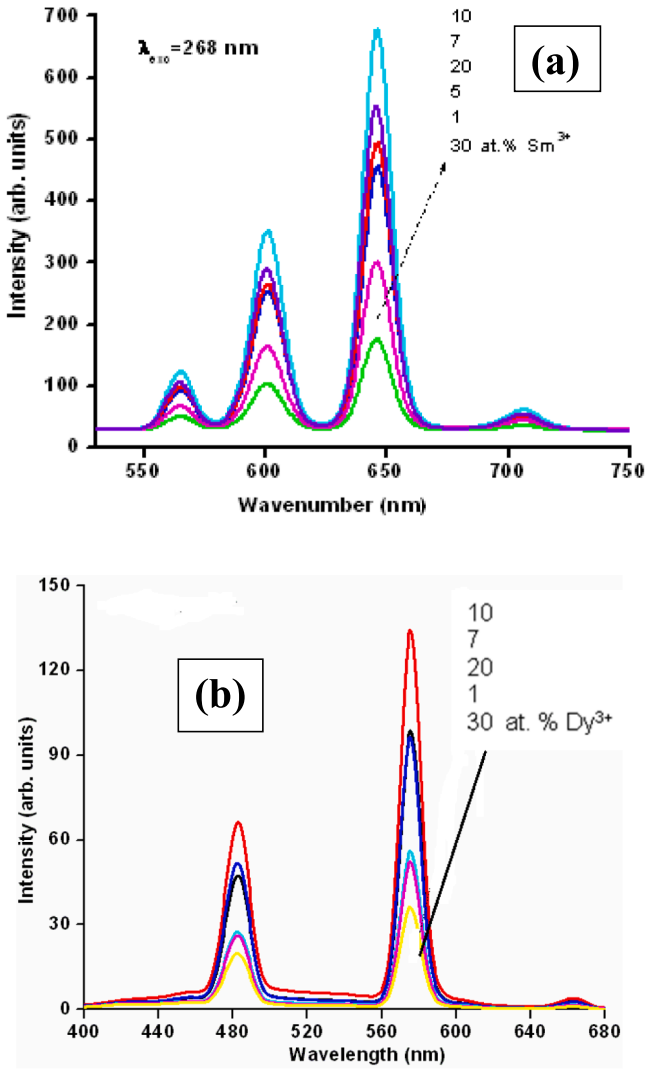

Fig. 6. (a) Emission spectra of Sm^{3+}- doped $BaMoO_4$ and (b) Emission spectra of Dy^{3+}- doped $BaMoO_4$ under excitation of 268 nm.

the FWHM of the curve, A_i the area under the curve, λ the wavelength and λ_{ci} the mean value corresponding to the transition. A_2 increases with Sm^{3+} and is maximum at 10 at.% and then decreases on increasing Sm^{3+} and, FWHM is found to be decrease from 12.6 to 11.3 nm as Sm^{3+} concentration increases upto 30 at.%. The highest luminescence intensity for $BaMoO_4$:Sm^{3+} and $BaMoO_4$:Dy^{3+} nanoparticles is found at 10 at.% Sm^{3+}/Dy^{3+} which is clearly shown in Fig. 6. Hence, the optimum concentration of Sm^{3+}/Dy^{3+} present in the $BaMoO_4$ host matrix is 10 at. % and it is considered as the critical concentration.

3.5.1. Determination of CIE coordinates

CIE chromaticity coordinates is the important property of the phosphors to determine its emission color. CIE coordinates have been determined for 10 at.% Sm^{3+} doped $BaMoO_4$ and for 10 at.% Dy^{3+} doped $BaMoO_4$ phosphor and found as (0.347, 0.463) for Sm^{3+}- doped $BaMoO_4$ and that of $BaMoO_4$:10Dy^{3+} is (0.436, 0.377) (Fig. 7). From this CIE coordinates, it is confirmed that Sm^{3+} -doped $BaMoO_4$ exhibit orange-red emission and that of Dy^{3+} doped $BaMoO_4$ exhibit yellowish green emission under UV excitation.

3.5.2. PVA composite film formation

Sm^{3+} and Dy^{3+} show its corresponding transitions after re-dispersing the samples in polar solvents such as water, ethanol, methanol etc. So, the prepared nanoparticles can be well re-dispersed and these nanoparticles can be used for the incorporation of luminescence materials in polymer matrix. The as prepared samples of $BaMoO_4$:Dy^{3+} (20 at. %) was further incorporated into polyvinyl alcohol to form thin polymer films. Excitation of Dy^{3+} in thin film of $BaMoO_4$ under 268 nm excitation also gives an intense yellow color (Fig. 8) which would find applications in biological assays and biological fluorescence labeling [26,27].

3.6. Decay lifetime study

The luminescence decay curve of $^4G_{5/2}$ level of Sm^{3+} and that $^4F_{9/2}$ level of Dy^{3+} have been taken for $BaMoO_4$:Sm^{3+} and $BaMoO_4$:Dy^{3+}. The excitation wavelength used is 268 nm. And that of emission wavelength used for Sm^{3+} and Dy^{3+} are 646 nm and 575 nm respectively. These experimentally observed decay curve are not well fitted by mono-exponential curve fitting. But all decay data (Fig. 9) are now well fitted into bi-exponential decay function, as

$$I = I_1 e^{-t/\tau_1} + I_2 e^{-t/\tau_2} \quad (4)$$

where I_1 and I_2 are the intensities at different time intervals and τ_1 and τ_2 their corresponding decay lifetimes. Then the average lifetime can be calculated as

$$\tau_{av} = \frac{I_1\tau_1^2 + I_2\tau_2^2}{I_1\tau_1 + I_2\tau_2} \quad (5)$$

This bi-exponential decay curve is observed when energy is transferred from donor/host to activator [17]. That is, energy is transfer from $BaMoO_4$ to Ln^{3+} in our study. This energy transfer process can be justified from the fact that lifetime of Sm^{3+}/Dy^{3+} decreases with the increase in Ln^{3+} contents. Fig. 9 shows the bi-exponential fitting to 7 at. % Sm^{3+} co-doped $BaMoO_4$. The longer lifetime is found at 10 at.% due to the absence of quenching effect (Fig. 10). This trend agrees well with the change of luminescence intensity with Ln^{3+} ions. Above 10 at.% decay lifetime decreases indicating the occurrence of concentration quenching. As the critical concentration is observed at 10 at.%, the concentration quenching occurs above 10 at.% Sm^{3+}/Dy^{3+} due to energy transfer from one activator to another activator until energy is absorbed. It is, therefore, required to obtain the critical distance (R_c) to justify the mechanism of energy transfer qualitatively. The critical distance between the donor (host) and the activator for energy transfer can be calculated using the equation proposed by Blasse's [28]:

$$R_c = 2\left[\frac{3V}{4\pi x_c N}\right]^{1/3} \quad (6)$$

here V is the unit cell volume, x_c is the critical concentration of Sm^{3+}/Dy^{3+} ion, and N is the number of cations in the host. For the present study, N = 1, V = 0.3826 nm^3 and x_c = 0.1 and the critical distance is found as 1.940 nm. Thus, the critical energy transfer distance is larger than the distance required for exchange interactions [29,30]. Therefore, the energy absorbed by the host is transferred to Ln^{3+} ions via multipolar interactions. This energy transfer through multipolar interaction may occur due to three possible multipolar mechanisms: dipole–dipole, dipole–quadrupole and quadrupole– quadrupole interactions [28]. According to the theory of Dexter, for the multipolar interactions, the dependence of luminescent intensity(I) on activator concentration can be expressed by the equation [31,32]:

$$\frac{I}{x} = K[1 + \beta(x)^{Q/3}]^{-1} \quad (7)$$

where × is the activator concentration (Sm^{3+}/Dy^{3+}). K and β are the constant for the same host under the same excitation condition. And Q values indicates the type of interactions such as the values of 6, 8 and 10 for dipole–dipole, dipole-quadrupole and quadrupole–quadrupole respectively [33–35]. The above equation can be simplified as by taking log of the equation (7)

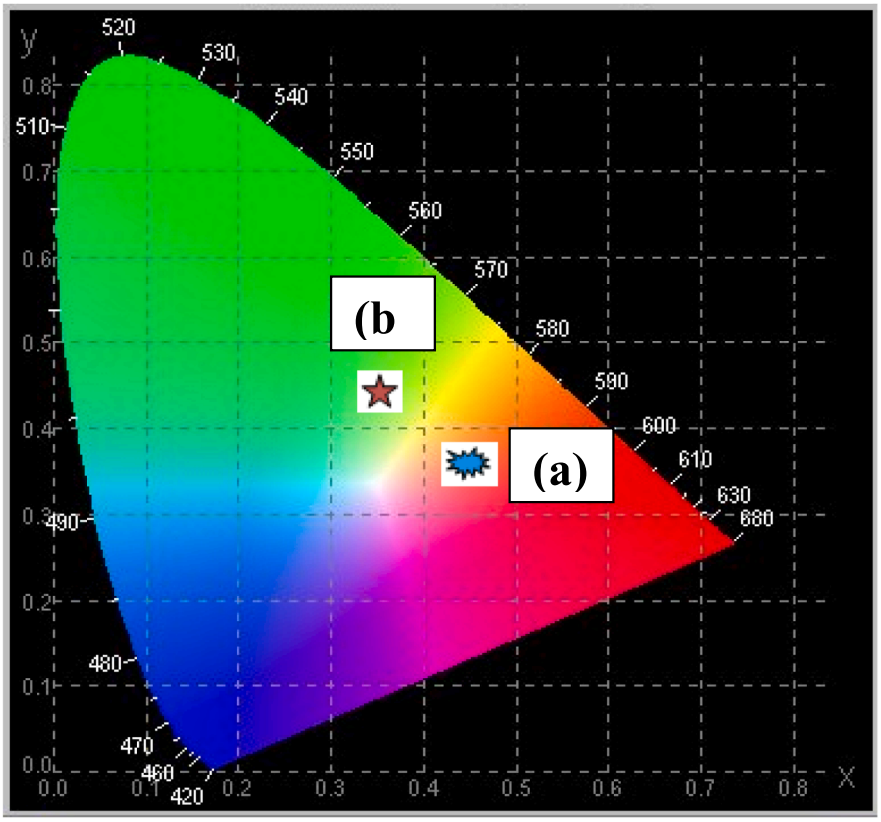

Fig. 7. CIE coordinates of (a) 10 at% Sm^{3+}-doped $BaMoO_4$ and (b) Dy^{3+} doped $BaMoO_4$.

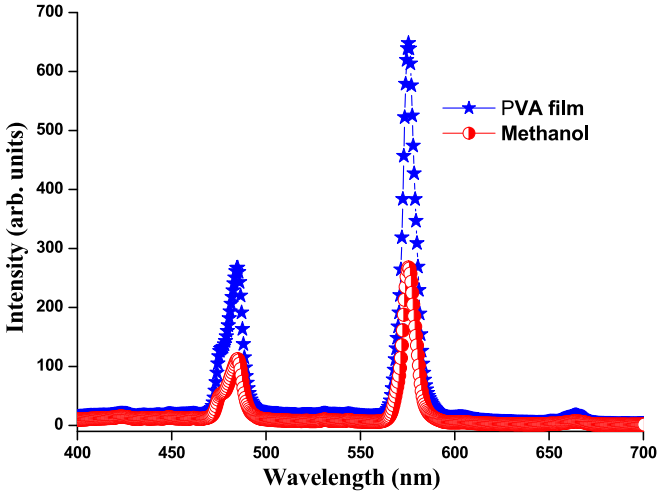

Fig. 8. Emission spectra of 5 at.% Dy^{3+} doped $BaMoO_4$ dispersed in PVA thin film and methanol.

$$\log\left(\frac{I}{x}\right) = \lg\frac{K}{\beta} - \frac{Q}{3}\lg x \tag{8}$$

Therefore, by plotting lg (I/x) vs lg ×, a curve is obtained with linear fitting of $R^2 = 0.9944$ and the slope of the curve is found to be – 1.686 (Fig. 11). Therefore, the value of Q is calculated as 5.64 which is closed to 6 indicating that the dipole–dipole interaction is the main mechanism of energy transfer among Ln^{3+} ions in $BaMoO_4$:Ln^{3+} (Ln^{3+} = Sm^{3+}/Dy^{3+}) phosphor. The rate of this energy transfer process increases with the increase of Ln^{3+} concentration, can be estimated by using the equation [36,37]

$$\eta_T = 1 - \frac{I}{I_o} \tag{9}$$

where η_T is the energy transfer efficiency, I and I_o are the emission intensities of the $BaMoO_4$ in the presence and absence of the activator (i.e. Sm^{3+}/Dy^{3+}), respectively. The energy transfer efficiency is found to be increased with rise in Sm^{3+}/Dy^{3+} contents reaching the maximum up to 85 % for × = 30 at.%. The calculated average life time values for $^4G_{5/2}$ levels are 0.62 ms and 0.82 ms for 5 and 7 at. % Sm^{3+} concentration. And, that of 5 and 7 at.% Dy^{3+} doped $BaMoO_4$ are 0.22 and 0.34 ms. This observed longer lifetime with Ln^{3+} ions is due to increase in crystallinity of the sample. These values are basically agrees well with other Sm^{3+} and Dy^{3+} doped luminescent phosphores [17,38,39].

4. Conclusion

Well-defined shuttle like $BaMoO_4$:Sm^{3+} and $BaMoO_4$:Dy^{3+}nanoparticles have been synthesized successfully by simple co-precipitation method. The structural properties and morphology of the host $BaMoO_4$ are not affected on doping the Ln^{3+} ions into the host. The PL emission spectra of both Sm^{3+} and Dy^{3+} are dominated by an electric-dipole transition over other transitions and their intensities are tuned on varying Ln^{3+} concentrations. The optimum concentration of Sm^{3+}/Dy^{3+} present in the $BaMoO_4$ host matrix is found to be 10 at.% and the dipole–dipole interaction is the dominant mechanism involved in energy transfer from donor to activator (Ln^{3+} = Sm^{3+}/Dy^{3+})ions. Under ultraviolet light excitation, the Sm^{3+}- doped $BaMoO_4$ phosphors show strong orange–red emission and $BaMoO_4$:Dy^{3+} show yellowish green

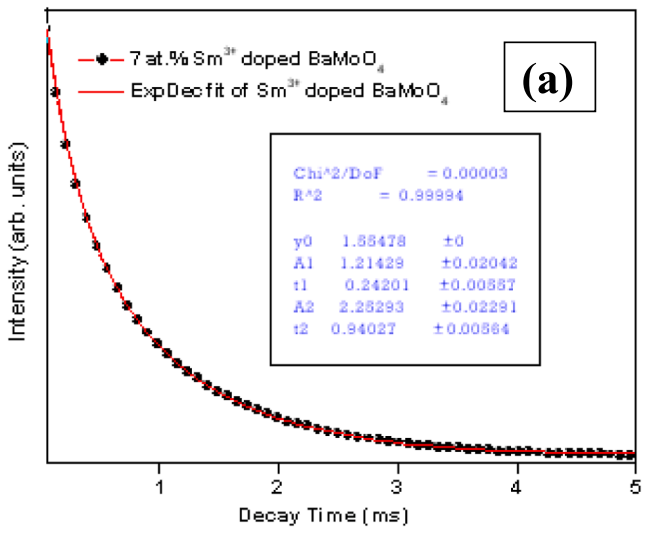

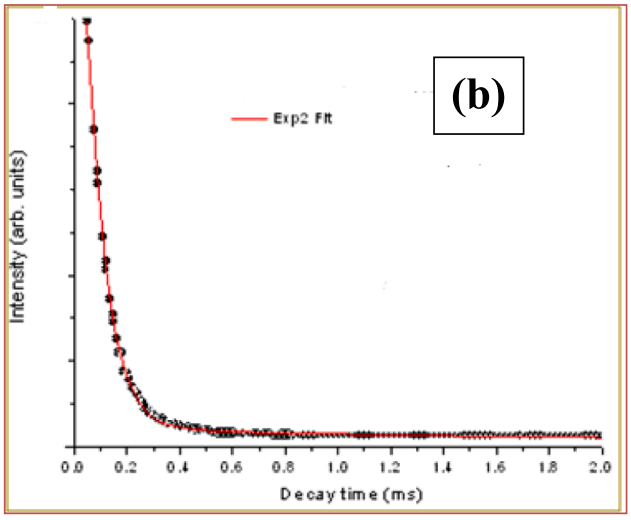

Fig. 9. Bi-exponential fitting to luminescence decay data of (a) 7at. % doped $BaMoO_4$:Sm^{3+} and (b) 7at. % doped $BaMoO_4$:Dy^{3+} nanoparticles.

emissions. And the prepared samples are incorporated into polyvinyl alcohol to form thin polymer films which on excitation under 268 nm gives an intense yellow color which would have great applications in biological fluorescence labeling.

CRediT authorship contribution statement

Ch. Victory Devi: Writing – original draft, Investigation, Writing – review & editing. **N. Rajmuhon Singh:** Writing – review & editing.

Declaration of Competing Interest

The authors declare that they have no known competing financial interests or personal relationships that could have appeared to influence the work reported in this paper.

Data availability

The data that has been used is confidential.

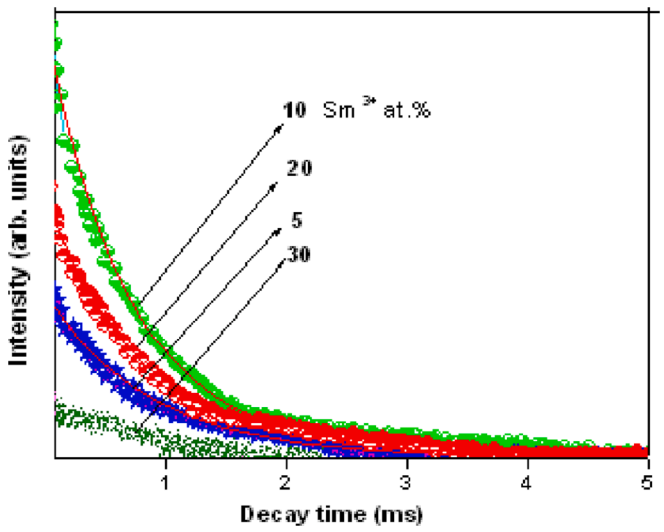

Fig. 10. Luminescence decay spectra of Sm^{3+}- doped $BaMoO_4$ nanoparticles at 268 nm excitation.

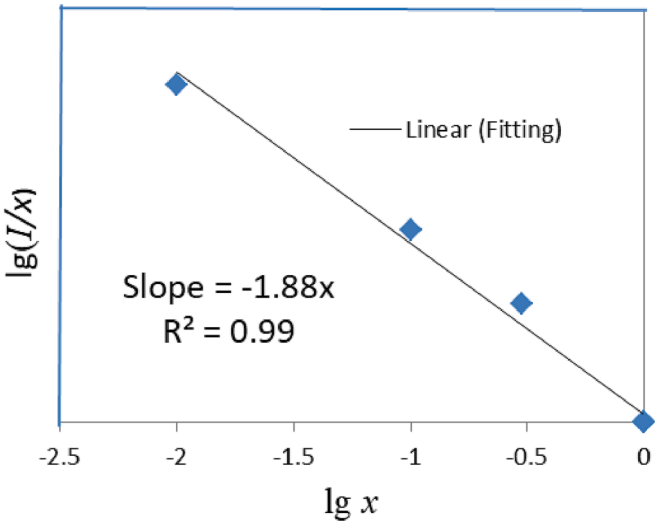

Fig. 11. The dependence of lg (I/x) on lg × according to Eq. (8).

Acknowledgements

Authors acknowledge UGC New Delhi, Govt. of India for receiving support under Minor research project.

References

[1] T. Justel, H. Nikol, C. Ronda, New development in the field of luminescent materials for lighting and displays, Angew. Chem. Int. Ed. (1998) 3084.
[2] A. Newport, J. Silver, A. Vecht, The Synthesis of Fine Particle Yttrium Vanadate Phosphors from Spherical Powder Precursors Using Urea Precipitation, J. Electrochem. Soc. 147 (2000) 3944–3951.
[3] C. Feldmann, T. Justel, C.R. Ronda, P.J. Schmidt, Inorganic Luminescent Materials: 100 Years of Research and Application, Adv. Funct. Mater. 13 (2003) 511.
[4] G. Li, Z. Wang, M. Yu, Z. Quan, J. Lin, Fabrication and optical properties of core–shell structured spherical SiO_2@$GdVO_4$:Eu^{3+} phosphors via sol–gel process, J. Solid State Chem. 179 (2006) 2698–2706.
[5] X. Liu, J. Lin, Nanocrystalline $LaGaO_3$:Tm^{3+} as an efficient blue phosphor for field emission displays with high color purity, Appl. Phys. Lett. 90 (2007) 184108–184115.
[6] C. Burda, X. Chen, R. Narayanan, M.A. El-Sayed, Chemistry and Properties of Nanocrystals of Different Shapes, Chem. Rev. 105 (2005) 1025–1102.
[7] Z.W. Pan, Z.R. Dai, Z.L. Wang, Nanobelts of Semiconducting Oxides, Science 291 (2001) 1947–1949.

[8] H.W. Chan, J.G. Duh, S.R. Sheen, $LiMn_2O_4$ cathode doped with excess lithium synthesized by co-precipitation for Li-ion batteries, J. Power Sources 115 (2003) 110.
[9] A.P. Kiselev, S.Z. Shmurak, B.S. Red'kin, V.V. Sinitsyn, I.M. Shmyt'ko, E. A. Kudrenko, E.G. Ponyatovskii, Evolution of the spectral response of amorphous europium molybdate under annealing, Phys. Solid State 48 (8) (2006) 1544.
[10] H. Canibano, G. Boulon, L. Palatella, Y. Guyot, A. Brenier, M. Voda, R. Balda, J. Fernandez, Spectroscopic properties of new Yb^{3+}-doped $K5Bi(MoO_4)_4$ crystals, J. Lumin. 102 (2003) 318.
[11] F.A. Kroger, Some Aspects of the Luminescence of Solids, Elsevier, Amsterdam, 1948.
[12] Y. Sun, J. Ma, J. Fang, C. Gao, Z. Liu, Synthesis of $BaMoO_4$ high photoluminescent whiskers by an electrochemical method. Ceramics International, Ceram. Int. 37 (2) (2011) 683–686.
[13] J.C. Sczancoski, L.S. Cavalcante, N.L. Marana, R.O. da Silva, R.L. Tranquilin, M. R. Joya, P.S. Pizani, J.A. Varela, J.R. Sambrano, M. Siu Li, E. Longo, J. Andre, Electronic structure and optical properties of BaMoO4 powders, Curr. Appl. Phys. 10 (2010) 614–624.
[14] X. Yang, Y. Zhou, X. Yu, H.V. Demir, X.W. Sun, Bifunctional highly fluorescent hollow porous microspheres made of $BaMoO_4$: Pr^{3+} nanocrystals via a template-free synthesis, J. Mater. Chem. 21 (2011) 9009–9013.
[15] L.S. Cavalcante, J.C. Sczancoski, R.L. Tranquilin, M.R. Joya, P.S. Pizani, J. A. Varela, E. Longo, $BaMoO_4$ powders processed in domestic microwave-hydrothermal: Synthesis, characterization and photoluminescence at room temperature, J. Phys. Chem. Solids 69 (2008) 2674–2680.
[16] M. Fujita, M. Itoh, T. Katagiri, D. Iri, M. Kitaura, V.B. Mikhailik, Optical anisotropy and electronic structures of $CdMoO_4$ and $CdWO_4$ crystals: Polarized reflection measurements, x-ray photoelectron spectroscopy, and electronic structure calculations, Phys. Rev. B 77 (2008), 155118.
[17] Ch. Victory Devi, Ganggam Phaomei, N. Yaiphaba , N. Rajmuhon Singh, Luminescence behavior of YVO_4:Dy^{3+} phosphors with enhanced photoluminescence on co-doping Bi^{3+} ions, J Alloys and Compd. 583(2014) 259-266.
[18] A.P.A. Marques, F.V. Motta, M.A. Cruz, J.A. Varela, E. Longo, I.L.V. Rosa, BaMoO4: Tb3 + phosphor properties: Synthesis, characterization and photophysical studiesSolid State, Ionics 202 (2011) 54–59.
[19] Y. Yin, Y. Li, H. Zhang, F. Ren, D. Zhang, W. Feng, L. Shao, K. Li, Y. Liu, Z. Sun, M. Li, G. Song, G. Wang, One-step fabrication of BaMoO4 microstructures with controlled morphologies via a simple EDTA-mediated routeSuperlattices, Microstruct. 55 (2013) 109–117.
[20] M.Y. William, Phosphor Handbook, CRC Press, 2006.
[21] A. Khanna, P.S. Dutta, $CaWO_4$: Eu^{3+}, Dy^{3+}, Tb^{3+} phosphor crystals for solid-state lighting applications, ECS Trans. 41 (2012) 39–48.
[22] Y. Su, L. Li, G. Li, Synthesis and Optimum Luminescence of CaWO4-Based Red Phosphors with Codoping of Eu3+ and Na+, Chem. Mater. 20 (2008) 6060–6067.
[23] F.B. Cao, L.S. Li, Y.W. Tian, Y.J. Chen, X.R. Wu, Investigation of red-emission phosphors (Ca, Sr) (Mo, W)O:Eu3+ crystal structure, luminous characteristics and calculation of Eu3+- 5D0 quantum efficiency, Thin Solid Films 519 (2011) 7971–7976.
[24] E. Cavalli, P. Boutinaud, R. Mahiou, M. Bettinelli, P. Dorenbos, Luminescence Dynamics in Tb^{3+}-Doped $CaWO_4$ and $CaMoO_4$ Crystals Inorg, Chem. 49 (2010) 4916–4921.
[25] A.K. Parchur, R.S. Ningthoujam, S.B. Rai, G.S. Okram, R.A. Singh, M. Tyagi, S. C. Gadkari, R. Tewari, R.K. Vatsa, Luminescence properties of Eu^{3+} doped $CaMoO_4$ nanoparticles, Dalton Trans. 40 (2011) 7595–7601.
[26] N. Yaiphaba, R. S. Ningthoujam, N. Shanta Singh, R. K. Vatsa, N. Rajmuhon Singh, Sangita Dhara, N. L. Misra, and R. Tewari, Luminescence, lifetime, and quantum yield studies of redispersible Eu^{3+}-doped $GdPO_4$ crystalline nanoneedles: Core-shell and concentration effects, Journal of Applied Physics 107 (2010) 034301-034310.
[27] A.K. Parchur, A.I. Prasad, A.A. Ansari, S.B. Rai, R.S. Ningthoujam, Luminescence properties of Tb^{3+}-doped $CaMoO_4$ nanoparticles: annealing effect, polar medium dispersible, polymer film and core–shell formation, Dalton Trans. 41 (2012) 11032–11045.
[28] G. Blasse, Energy transfer in oxidic phosphors, Phys. Lett. A 28 (1968) 444–445.
[29] X.G. Zhang, L.Y. Zhou, Q. Pang, M.L. Gong, Novel broadband excited and linear red-emitting $Ba_2Y(BO_3)_2Cl$:Ce^{3+}, Tb^{3+}, E^{u3}+ phosphor: luminescence and energy transfer, J. Am. Ceram. Soc. 97 (2014) 2124–2131.
[30] Y. Zaifa, S. Yumei, X. Qiguang, S. Jiayue, Preparation and photoluminescence properties of Dy^{3+}-doped $Ba_3Lu(PO_4)_3$ phosphors, J. Rare Earths 33 (2015) 1251–1255.
[31] D.W. Wen, G.H. Yang, H. Yang, J.X. Shi, M.L. Gong, M. Wu, Photoluminescence properties of color-tunable novel $Na_2Ca_4(PO_4)2SiO_4$:Ce^{3+}, T^{b3}+ near ultraviolet convertible phosphors, Mater. Lett. 63 (2014) 125–130.
[32] D.L. Dexter, A theory of sensitized luminescence in solids, J. Chem. Phys. 21 (1953) 836–850.
[33] W.Z. Lv, Y.C. Jia, Q. Zhao, M.M. Jiao, B.Q. Shao, W. Lu, H.P. You, Color tuning and energy transfer investigation in $Na_2Ca_4Mg_2Si_4O_{15}$:Eu^{2+}, Mn^{2+} phosphor and its potential application for UV-excited UV-WLEDs, RSC Adv. 15 (2014) 7588–7593.
[34] D.L. Monika, H. Nagabhushana, R.H. Krishna, B.M. Nagabhushana, S.C. Sharma, T. Thomas, Synthesis and photoluminescence properties of a novel Sr_2CeO_4:Dy^{3+} nanophosphor with enhanced brightness by Li^+ co-doping, RSC Adv. 73 (2014) 38655–38659.
[35] X.G. Zhang, J.L. Zhang, Z.Y. Dong, J.X. Shi, M.L. Gong, Concentration quenching of Eu^{2+} in a thermal-stable yellow phosphor Ca_2BO_3Cl:Eu^{2+} for LED application, J. Lumin. 132 (2012) 914–918.
[36] S.H. Lee, Y. Cha, H. Kim, S. Lee, J.S. Yu, Luminescent properties of Eu^{3+}-activated Gd_2ZnTiO_6 double perovskite red-emitting phosphors for white light-emitting diodes and field emission displays, RSC Adv. 8 (2018) 11207–11215.
[37] T. Yaba, R. Wangkhem, N. Shanta Singh, Enhanced red emission from Bi^{3+} sensitized $CaWO_4$:Eu^{3+} as red component for near UV/blue LED pumped white light emission, 843 (2020) 156022–156032.
[38] P. Yang, C. Li, W. Wang, Z. Quan, S. Gai, J. Lin, Uniform $AMoO_4$: Ln (A=S^{r2}+, B^{a2}_{+}; Ln=E^{u3}+, T^{b3}+) submicron particles: Solvothermal synthesis and luminescent properties, J. Solid State Chem. 182 (2009) 2510–2523.
[39] S. Sailaja, S.J. Dhoble, B.S. Reddy, Synthesis and photoluminescence properties of Sm^{3+} and Dy^{3+} ions activated $Ca_2Gd_2W_3O_{14}$ phosphors, J. Mol. Struct. 1003 (2011) 115–124.